

Encapsulating high-temperature superconducting twisted van der Waals heterostructures blocks detrimental effects of disorder

Yejin Lee,^{1,2} Mickey Martini,^{1,2} Tommaso Confalone,^{1,3} Sanaz Shokri,^{1,2}
Christian N. Saggau,¹ Genda Gu,⁴ Kenji Watanabe,⁵ Takashi Taniguchi,⁶ Domenico
Montemurro,⁷ Valerii M. Vinokur,⁸ Kornelius Nielsch,^{1,2,9} and Nicola Poccia^{*1}

¹*Leibnitz Institute for Solid State and Materials Science Dresden (IFW Dresden), 01069 Dresden, Germany*

²*Institute of Applied Physics, Technische Universität Dresden, 01062 Dresden, Germany*

³*Department of Physics, Sapienza University of Rome, 00185 Rome, Italy*

⁴*Condensed Matter Physics and Materials Science Department,
Brookhaven National Laboratory, Upton, NY 11973, USA*

⁵*Research Center for Functional Materials, National Institute for Materials Science, 1-1 Namiki, Tsukuba 305-0044, Japan*

⁶*International Center for Materials Nanoarchitectonics,
National Institute for Materials Science, 1-1 Namiki, Tsukuba 305-0044, Japan*

⁷*Department of Physics, University of Naples Federico II, 80125 Naples, Italy*

⁸*Terra Quantum AG, 9400 Rorschach, Switzerland*

⁹*Institute of Materials Science, Technische Universität Dresden, 01062 Dresden, Germany
(*n.poccia@ifw-dresden.de)*

(Dated: October 6, 2022)

High-temperature cuprate superconductors (HTS)-based van der Waals (vdW) heterostructures hold high technological promise. One of the obstacles hindering progress is the detrimental effect of disorder on the properties of Josephson junctions (JJ) realized by the vdW devices. Here we report the new method of fabricating twisted vdW heterostructures made of $\text{Bi}_2\text{Sr}_2\text{CuCa}_2\text{O}_{8+\delta}$, crucially improving the JJ characteristics, pushing them up to those of the intrinsic JJs in bulk samples. The method combines a cryogenic stacking using a solvent-free stencil mask technique and covering interface by the insulating hexagonal boron nitride crystals. Despite the high-vacuum condition down to 10^{-6} mbar in the evaporation chamber, the interface appears to be protected from water molecules during the in-situ metal deposition only when fully encapsulated. Comparing the current-voltage curves of encapsulated and unencapsulated interfaces, we reveal that the encapsulated interfaces' characteristics are crucially improved so that the corresponding JJs demonstrate high critical currents and sharpness of the superconducting transition comparable to those of the intrinsic JJs. Finally, we show that the encapsulated heterostructures are more stable in time.

Keywords: Van der Waals heterostructures, twisted high temperature superconductors, Josephson junctions, 2D materials

I. INTRODUCTION

Layered quasi-two dimensional (2D) materials comprising the stack of monolayers held together by van der Waals forces can be cleaved via a simple scotch tape exfoliation down to a constitutive monolayer [1]. Layered high temperature superconductors (HTSC) provide a wide variety of such correlated systems. Remarkably, even the atomically thin $\text{Bi}_2\text{Sr}_2\text{CuCa}_2\text{O}_{8+\delta}$ (BSCCO) layers have been found to possess the superconducting transition temperature close to that of the bulk samples [2, 3] and showed the superconductor-insulator transition driven by the evolution of the density of states [4]. Because of these properties, HTSCs can serve as starting building blocks for the vdW heterostructures. However, isolating cuprate single layers that hold superconductivity remains a challenging task, especially if one wishes to realise atomically thin and crystalline-ordered interfaces. The point is that the atomically thin BSCCO flakes turn highly insulating if contaminated with oxygen under the ambient atmosphere [1, 5]. Raman measurements [5, 6] reported high chemical activity of oxy-

gen in thin BSCCO flakes. More detailed studies [7] revealed that water molecules can also quickly deteriorate the surface of BSCCO flakes. In addition, oxygen dopants in cuprates are mobile above 200 K [8, 9], destroying high quality superconductivity requiring ordered distribution of oxygen defects [10, 11]. In comparison with the bulk crystalline order, the robustness of the spatially-correlated superlattice orders in BSCCO down to few unit cells is remarkable [12]. Thus, cryogenic temperatures and the well-controlled environment are necessary to prevent detrimental disorder in the spatially correlated superlattices and to freeze oxygen defects in their functional original positions for realizing the quality cuprates-based vdW heterostructures.

The possibility of making the twisted HTSC-based heterostructures has attracted substantial interests because of the d -wave pairing symmetry [13]. Previous twisted BSCCO junctions using bulk crystals or flakes were realized through an annealing process at high temperature in oxygen atmosphere [14, 16], which can reconstruct the interfacial structure [15]. The obtained structures did not demonstrate any angular dependence of the Josephson current [14, 16]. Nevertheless, the non-monotonic an-

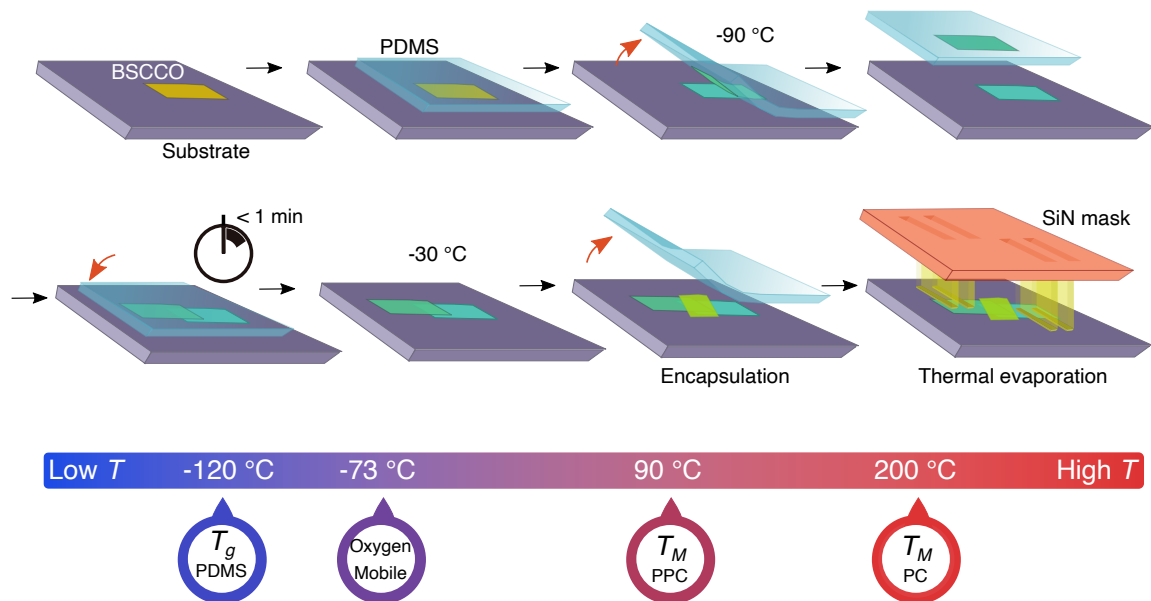


FIG. 1. Cryogenic fabrication process for BSCCO junctions. An exfoliated BSCCO flake is identified by its optical contrast under a microscope and a PDMS stamp is approached towards the flake on the substrate. The cold PDMS stamp is dragged, cleaving the crystal at $-90\text{ }^{\circ}\text{C}$ and then quickly aligned along the flake. Stacked flakes are slowly warmed to $-30\text{ }^{\circ}\text{C}$, and the PDMS is pulled off. The junction interface is covered by landing a hBN flake using a PDMS at room temperature. Electrical contacts on the crystals are deposited by thermal evaporation through a SiN stencil mask. The color bar below indicates representative temperatures for oxygen in cuprates and different types of polymer (PDMS, PPC and PC).

gular behavior of the critical current has been reported on the cross-whisker HTSCs junctions, with the critical current being much reduced as compared to the critical current of the bulk intrinsic junctions [17]. On the other hand, the angular dependence in cuprate in-plane grain boundary junctions is well described by the d -wave pairing symmetry because of the larger coherence length as compared to that in out-of-plane junctions [18, 19], which reduces the detrimental disorder effects. However, transmission electron microscopy has shown that the grain-boundary Josephson junctions (GBJJs) are generally composed of facets in the range of 10–100 nm that strongly depend on the particular HTS material, the substrate, the conditions of the film deposition, and on the presence of defects [20]. Facets could take place in all three dimensions as a consequence of the adopted fabrication techniques for bicrystals, bi-epitaxial growth, or step edges [21]. The GBJJs have been well studied, and their electronic properties were found to be controlled by the misorientation between two grains [22]. Because of that, the facets create additional complexity and difficulties for controlling the JJs properties.

An angular dependence of currents in out-of-plane Josephson junction resulting in its change over two orders of magnitude has been demonstrated in thin BSCCO twisted heterostructures prepared by the cryogenic stacking technique, while preserving the coherence of the crystalline and oxygen order at the interface [23]. An additional important evidence of the significant reduction of the Josephson current when changing the twist angle

has been reported in [24]. It was found that the corresponding critical currents are, on average, lower than the critical current of an intrinsic Josephson junction for the BSCCO as compared to the magnitudes measured in [23], given that the fabrication did not occur under the cryogenic condition. Because of the general improvement in the control of the BSCCO in the low-dimensional limit, there has been a flourishing of theoretical activities. The emergence of the topological states in twisted vdW heterostructures of HTS BSCCO layers with the d -wave superconducting order parameter was viewed as a realistic possibility [25–30]. The twist angle close to 45° was found to result in a time reversal symmetry (TRS) broken chiral superconducting $d_{x^2-y^2} \pm id_{xy}$ phase which was also reported at the intermediate twist angles and was attributed to the unconventional sign structure of the d -wave order parameter [26, 31]. Strong support for this theoretical proposal came from the experimental detection of some new interfacial superconductivity [23], manifesting as a dominant second harmonic of the Josephson current close to 45° angle. However, the TRS breaking in the high temperature superconducting phase can be suppressed by strong disorder at the interface [31], hence careful studies of detrimental disorder effects on the interfaces and novel methods that rely on cheaper and/or innovative process of fabrication are required.

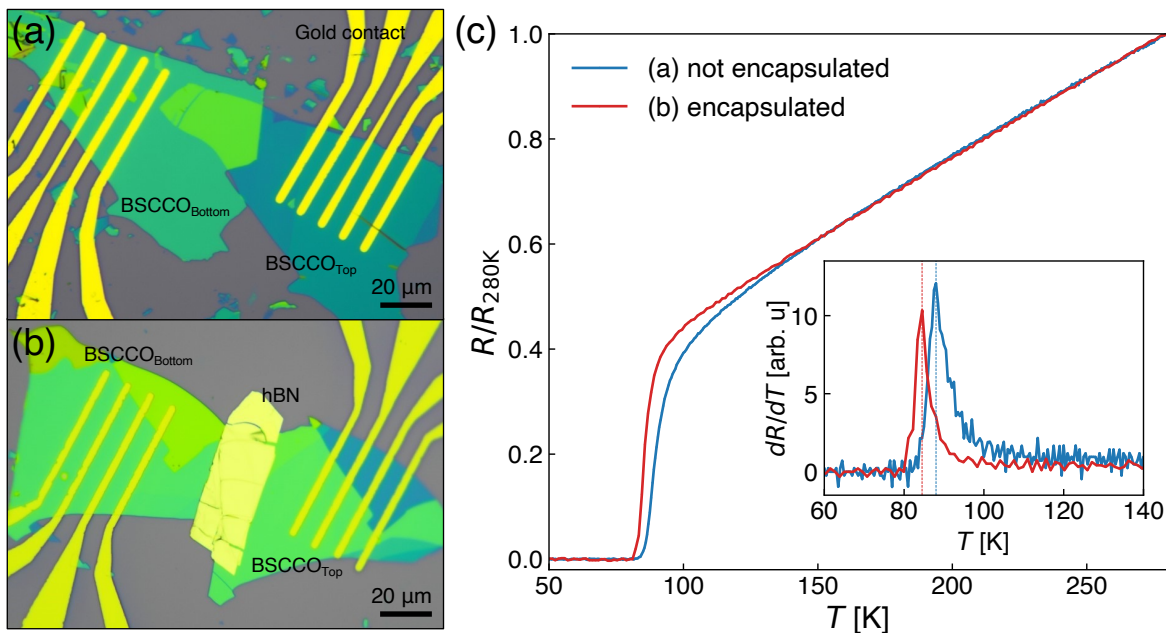


FIG. 2. (a) Optical micrograph of BSCCO junctions with uncovered interface and (b) hBN-encapsulated interface. (c) Normalized resistance $R/R_{280\text{K}}$ as a function of temperature T of BSCCO junctions corresponding in (a) and (b), respectively. Inset of (c): The derivative dR/dT as a function of temperature. The dotted lines shows superconducting critical temperature T_c for junctions with an encapsulating crystal (red) and without encapsulation (blue).

II. FABRICATION

We fabricate Josephson junctions based on the optimally doped BSCCO flakes using a cryogenic dry transfer technique in a pure argon atmosphere. This technique consists of cleaving a sequential pair of fresh surfaces of the BSCCO from the pre-exfoliated single crystal and stacking the two resulting flakes on top of each other. This procedure of the junction fabrication is sketched in Fig. 1 and can be described as follows. First, the BSCCO crystals are mechanically exfoliated using a scotch tape on the SiO_2/Si substrates, previously treated with oxygen plasma and baked overnight to get rid of water molecules. Next, utilising the optical contrast we identify a BSCCO flake with the thickness in the range between 80 and 100 nm, and cool the sample stack down to -90°C , to preserve the crystalline structure and the superconducting state of the interface while building the junction. After that, we cover the BSCCO flake with an edge of a polydimethylsiloxane (PDMS) stamp placed on a glass slide mounted on a micromanipulator and let the assembly thermalize. At that temperature, which is a little above the glass transition of our PDMS ($T_g = -120^\circ\text{C}$), the stamp becomes very adhesive. By quickly detaching the stamp from the substrate, we cleave the crystal along an atomically flat plane between BiO planes, obtaining two thinner flakes. The flake standing on the PDMS stamp is aligned and placed back onto the bottom flake on the substrate within 90 seconds. The time between cleaving and stacking makes a huge

impact on the junction quality. We find out that both flakes should be thicker than 30 nm, otherwise they are not rigid enough to create a flat interface without modulating the surface. Finally, the stage is slowly heated up to -30°C and the top flake is released on the bottom one as the stamp is no longer adhesive. In Figure 1, the bottom color bar illustrates representative temperatures (eg. melting temperature T_M) of the commonly used polymers for exfoliation such as polycarbonate(PC) and polypropylene carbonate(PPC)[32]. The control over adhesion of the PDMS stamp allows us to fabricate the junctions by taking advantage of a solvent free and dry transfer at low temperature.

For one of the two junctions considered in this study, we opt to additionally protect the interface especially from water molecules by placing an encapsulating hexagonal boron nitride (hBN) flake on top of the stacked flakes immediately afterwards. Electrical contacts are then deposited in two steps using a chemical-free stencil mask technique[3] in an evaporation chamber, directly connected to the glovebox cluster. First, gold electrodes are evaporated right on the junctions while the temperature of the liquid nitrogen-cooled stage is kept at -50°C . The base pressure of the deposition chamber is 10^{-6} mbar. Next, electrical contact pads are deposited via stencil masks by evaporating Au/Cr while the temperature of the sample stage is -30°C . This double evaporation aims to avoid deposition of the Cr directly onto the BSCCO, which would result in an insulating behavior of the underlying region, as Cr could capture oxygen atoms from the flakes [33]. We found that the contact resistance ob-

tained from a deposition of Cr right onto the sample by performing a single evaporation (Au/Cr) was of the order of $1\text{ k}\Omega$, which is ten times higher than the resistance of the contact obtained by the two-steps evaporation protocol.

Figure 2(c) shows the temperature, T , dependence of the electrical resistance normalized by the resistance at 280 K for two devices, one with a hBN encapsulation on top of the junction (Fig. 2(a)) and the other without it Fig. 2(a). The dependence is linear in the normal state, consistent with the nearly optimal doped $\text{Bi}_2\text{Sr}_2\text{CuCa}_2\text{O}_{8+\delta}$ [34] and exhibits a superconducting transition, at temperature slightly lower than that of the bulk samples [35]. The superconducting critical temperature T_c in the junction with the encapsulated (uncovered) interface is 84.5 K (88 K), defined as the peak value in the derivative dR/dT (Fig. 2(c)). The T_c is close to that of a bulk crystal, indicating the high uniformity of oxygen dopants even at the junction in both of the devices, and its values are within the distribution of T_c in twisted BSCCO junctions[23]. Yet, the device with the encapsulated junction displays a visibly sharper transition from the resistive to metallic state, indicating the improved interplanar coupling [36].

III. RESULTS AND DISCUSSION

The current voltage, I - V , characteristics and the dynamical resistance, dV/dI , across the JJ are measured in a four terminal device configuration using a lock-in amplifier technique. We sweep the dc current from negative to positive values in the range of mA, while superimposing the small alternating current with an $1\text{ }\mu\text{A}$ -amplitude and a frequency of 17 Hz. We measure simultaneously the dc and ac voltages to get the I - V and dV/dI characteristics, respectively. To compare transport data of the two JJs, we normalize the bias current I with respect to the junction area A obtaining the current density $j = I/A$. Figure 3(a) displays the representative j - V characteristics of the BSCCO junction without encapsulation at 5 K and 50 K. The schematic of the device is sketched in the inset of Fig. 3(a). As we sweep the bias current from a large negative value, the junction voltage first retraps to the superconducting state, $V = 0$, and then jumps to the resistive state at the critical current density j_c . In this JJ, $j_c = 0.10\text{ kA/cm}^2$ at 5 K and decreases to $j_c = 0.06\text{ kA/cm}^2$ at 50 K.

Figure 3(b) shows the differential resistance dV/dI as a function of the current density and temperature. The critical current density j_c at which the inner peaks of dV/dI appear, decreases with temperature. Furthermore, multiple peaks are visible at higher bias current (for both bias polarities) above 25 K approximately. These features possibly arise from the subgap structure of the quasiparticle density of states in the intrinsic BSCCO Josephson junctions [37, 38]. The dV/dI is symmetric with respect to $j = 0$.

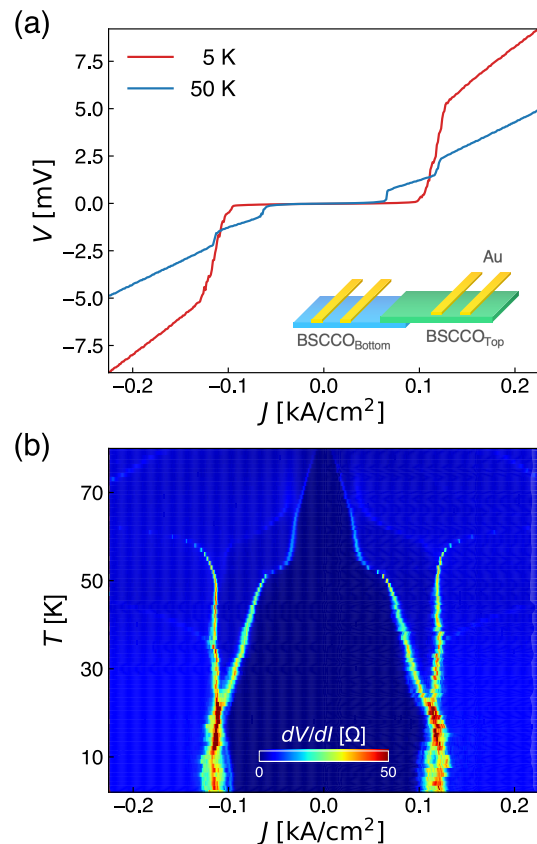


FIG. 3. (a) Representative current density-voltage J - V characteristics at 5 K and 50 K, and (b) differential resistance as a function of current density and temperature of the BSCCO junction without encapsulation on the interface. Inset of (a): Schematic illustration of corresponding BSCCO junction.

The j - V characteristics of the junction with encapsulated interface measured at 5 K and 50 K are presented in Fig. 4(a). The sketch of the corresponding device is displayed in the inset of Fig. 4(a). The transition from the superconducting to resistive state occurs at the current density almost ten times higher than that of the former junction ($j_c = 1.19\text{ kA/cm}^2$ at 5 K). This value is comparable with the j_c of intrinsic BSCCO Josephson junctions, which ranges from 0.17 to 1.70 kA/cm^2 at 10 K, depending on the number of junctions along the c -axis [39]. This JJ exhibits a sharp transition where the system rapidly jumps at j_c from zero voltage to a finite voltage of 20 mV at 5 K, while it ends up to a voltage of 2 mV at 50 K. This suggests that the superconducting gap decreases by the order of magnitude when the temperature raises from 5 K to 50 K, as the switching voltage corresponds to the superconducting gap values in ideal tunnel junctions [40]. Furthermore, the j - V curve at 50 K displays additional voltage jumps when the current density exceeds the j_c . This suggests the contribution of each intrinsic junction in crystals in the framework of Resistively and capacitively shunted junction (RCSJ) model using two resistance in series.[41]. To gain further insight, we plot in

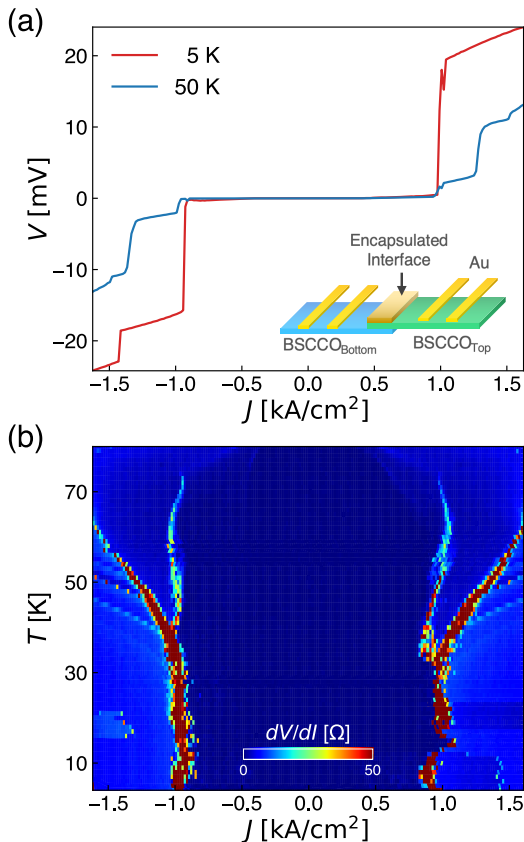


FIG. 4. (a) Representative current-voltage characteristics at 5 K and 50 K. (b) Differential resistance versus current density and temperature of the BSCCO junction with the encapsulated interface. Inset of (a): Corresponding schematics of BSCCO junction with the encapsulated interface.

Fig. 4(b) the dV/dI of the encapsulated JJ versus current density and temperature. The first peaks of dV/dI occurring at j_c exhibit a non-monotonic behavior as a function of temperature. In this case, j_c is not mirrored along $j = 0$ below 40 K, and small hysteretic behavior is presented. Namely, the current density at which the junction re-traps to the zero resistance state from the negative bias is slightly lower than the current density at which the system jumps to the resistive state at the positive bias. Above 40 K, dV/dI is symmetric and several peaks can be identified above j_c . These features appear at different current density depending on the temperature and can be associated either with the subgap structure as in the previous case [37, 38], the formation of the discrete vortex train [42], or with the multiparticle tunneling mechanisms [43], such as phonon assisted tunneling process [44, 45]. These structures in the subgap regime are well explained by the resonant coupling mechanism between the infrared active optical c -axis phonons and oscillating Josephson currents [44]. When the bias is much higher than the critical current, no structures are presented, and the j - V characteristic is linear. Taking advantage of the linear behavior, we estimate the normal

resistance R_n , defined as the slope of the voltage curve with respect to the current in the linear regime right below T_c . Then we use this R_n as an additional yardstick to compare the two devices. We quantify $R_{n1} = 4.2 \Omega$ and $R_{n2} = 4.6 \Omega$ for the junctions without and with encapsulation, respectively, despite the difference in the junction area ($670 \mu\text{m}^2$ and $120 \mu\text{m}^2$).

IV. CONCLUSION

In summary, we have investigated the detrimental effects of disorder on electronic transport of JJs based on stacked BSCCO heterostructures and demonstrated the improvement of the corresponding I - V characteristics and the dV/dI due to encapsulated interface with an hBN-crystal, fabricated using cryogenic, solvent-free transfer techniques in Ar atmosphere. Encapsulation of the junction interface is, under our experimental conditions, of the vital importance for the fabrication of JJs with an electronic quality comparable to intrinsic Josephson junctions in single-crystal BSCCO. Our main finding is that j_c is high in the encapsulated JJ as high as in the intrinsic junction ($j_c \sim 1.2 \text{ kA/cm}^2$ at 10 K), whereas j_c in the not-encapsulated JJ is about an order of magnitude small. The sharper transition in the $R(T)$, the presence of structures and hysteresis in the I - V characteristics observed in the encapsulated device coincide with the main features of the coherent JJ free of detrimental disorder making it an excellent platform for applications.

Acknowledgements. The experiments were partially supported by the Deutsche Forschungsgemeinschaft (DFG 452128813, DFG 512734967, DFG 492704387, DFG 460444718). The work of V.M.V. was supported by the Terra Quantum AG. The authors are grateful to Heiko Reith and Nicolas Perez Rodriguez for providing access to cleanroom and cryogenic facilities respectively. K.W. and T.T. acknowledge support from the JSPS KAKENHI (Grant Numbers 19H05790, 20H00354 and 21H05233). The work at BNL was supported by the US Department of Energy, office of Basic Energy Sciences, contract no. DOE-sc0012704. The authors are also grateful to S. Y. Frank Zhao, Philip Kim, Francesco Tafuri, Giampiero Pepe; Naurang Lal Saini and Valentina Brosco for illuminating and fruitful discussions.

Author contributions. N.P. conceived and designed the experiment; Y.L., M.M. performed the experiments and analyzed the data with the contribution of T.C., S.S., C.N.S. The cuprate crystals have been provided by G.G. The hexagonal boron nitride crystals have been provided by K.W. and T.T. The fabrication procedure and the results have been discussed by N.P., Y.L., M.M. and V.M.V. The manuscript has been written by N.P., Y.L., M.M., D.M., V.M.V., and K.N. All authors

discussed the manuscript.

Conflict of Interest All authors declare no conflict of interest.

-
- [1] K. S. Novoselov, D. Jiang, F. Schedin, T. Booth, V. Khotkevich, S. Morozov, and A. K. Geim, *Proc. Natl. Acad. Sci. U.S.A.* **2005**, *102*, 10451-10453.
- [2] Y. Yu, L. Ma, P. Cai, R. Zhong, C. Ye, J. Shen, G. D. Gu, X. H. Chen, Y. Zhang, *Nature* **2019**, *575*, 156-163.
- [3] S. F. Zhao, N. Poccia, M. G. Panetta, C. Yu, J. W. Johnson, H. Yoo, R. Zhong, G. Gu, K. Watanabe, T. Taniguchi, S. V. Postolova, V. M. Vinokur, P. Kim, *Phys. Rev. Lett.* **2019**, *122*, 247001.
- [4] M. Liao, Y. Zhu, J. Zhang, R. Zhong, J. Schneeloch, G. Gu, K. Jiang, D. Zhang, X. Ma, Q.-K. Xue, *Nano Lett.* **2018**, *18*, 5660-5665.
- [5] L. Sandilands, A. Reijnders, A. Su, V. Baydina, Z. Xu, A. Yang, G. Gu, T. Pedersen, F. Borondics, K. Burch, *Phys. Rev. B* **2014**, *90*, 081402.
- [6] L. Sandilands, J. Shen, G. Chugunov, S. Zhao, S. Ono, Y. Ando, K. Burch, *Phys. Rev. B* **2010**, *82*, 064503.
- [7] Y. Huang, L. Zhang, X. Zhou, L. Liao, F. Jin, X. Han, T. Dong, S. Xu, L. Zhao, Y. Dai, Q. Cheng, X. Huang, Q. Zhang, L. Wang, N.-L. Wang, M. Yue, X. Bai, Y. Li, Q. Wu, H.-J. Gao, G. Gu, Y. Wang, X.-J. Zhou, *ACS Appl. Mater. Interfaces* **2022**.
- [8] M. Fratini, N. Poccia, A. Ricci, G. Campi, M. Burghammer, G. Aeppli, A. Bianconi, *Nature* **2010**, *466*, 841-844.
- [9] N. Poccia, M. Fratini, A. Ricci, G. Campi, L. Barba, A. Vittorini-Orgeas, G. Bianconi, G. Aeppli, A. Bianconi, *Nat. Mat.* **2011**, *10*, 733-736.
- [10] N. Poccia, A. Ricci, G. Campi, M. Fratini, A. Puri, D. D. Gioacchino, A. Marcelli, M. Reynolds, M. Burghammer, N. L. Saini, G. Aeppli, A. Bianconi, *Proc. Natl. Acad. Sci. U.S.A.* **2012**, *109*, 15685-15690.
- [11] G. Campi, A. Bianconi, N. Poccia, G. Bianconi, L. Barba, G. Arrighetti, D. Innocenti, J. Karpinski, N. D. Zhigadlo, S. M. Kazakov, M. Burghammer, M. v. Zimmermann, M. Sprung, A. Ricci, *Nature* **2015**, *525*, 359-362.
- [12] N. Poccia, S. Y. F. Zhao, H. Yoo, X. Huang, H. Yan, Y. S. Chu, R. Zhong, G. Gu, C. Mazzoli, K. Watanabe, T. Taniguchi, G. Campi, V. M. Vinokur, P. Kim *Phys. Rev. Mater.* **2020**, *4*, 114007.
- [13] R. Klemm, C. Rieck, and K. Scharnberg, *Phys. Rev. B* **2000**, *61*, 5913.
- [14] Y. Zhu, M. Liao, Q. Zhang, H.-Y. Xie, F. Meng, Y. Liu, Z. Bai, S. Ji, J. Zhang, K. Jiang, R. Zhong, J. Schneeloch, G. Gu, L. Gu, X. Ma, D. Zhang, Q.-K. Xue, *Phys. Rev. X* **2021**, *11*, 031011.
- [15] Y. Zhu, Q. Li, Y. Tsay, M. Suenaga, G. Gu, N. Koshizuka, *Phys. Rev. B* **1998**, *57*, 8601.
- [16] Q. Li, Y. Tsay, M. Suenaga, R. Klemm, G. Gu, N. Koshizuka, *Phys. Rev. Lett.* **1999**, *83*, 4160.
- [17] Y. I. Latyshev, A. Orlov, A. Nikitina, P. Monceau, R. Klemm, *Phys. Rev. B* **2004**, *70*, 094517.
- [18] J. Mannhart, H. Hilgenkamp, G. Hammerl, C. W. Schneider, *Phys. Scr.* **2002**, *2002*, 107.
- [19] H. Hilgenkamp, J. Mannhart, Grain boundaries in high-T_c superconductors. *Rev. Mod. Phys.* **2002**, *74*, 485.
- [20] R. Baghdadi, R. Arpaia, E. Stepantsov, M. Arzeo, D. Golubev, D. Montemurro, E. Andersson, T. Bauch, F. Lombardi, *Phys. Rev. B* **2017**, *95*, 184505.
- [21] H. Hilgenkamp, J. Mannhart, B. Mayer, *Phys. Rev. B* **1996**, *53*, 14586.
- [22] D. Dimos, P. Chaudhari, J. Mannhart, and F. LeGoues, *Phys. Rev. Lett.* **1988**, *61*, 219.
- [23] S. Zhao, N. Poccia, X. Cui, P. A. Volkov, H. Yoo, R. Engelke, Y. Ronen, R. Zhong, G. Gu, S. Plugge, T. Tummuru, M. Franz, J. H. Pixley, P. Kim, *ArXiv Preprint arXiv:2108.13455* **2021**.
- [24] J. Lee, W. Lee, G.-Y. Kim, Y.-B. Choi, J. Park, S. Jang, G. Gu, S.-Y. Choi, G. Y. Cho, G.-H. Lee, H.-J. Lee *Nano Lett.* **2021**, *21*, 10469-10477.
- [25] O. Can, X.-X. Zhang, C. Kallin, M. Franz, *Phys. Rev. Lett.* **2021**, *127*, 157001.
- [26] T. Tummuru, S. Plugge, M. Franz, *Phys. Rev. B* **2022**, *105*, 064501.
- [27] T. Tummuru, E. Lantagne-Hurtubise, M. Franz, *ArXiv Preprint arXiv:2202.08790* **2022**.
- [28] A. Mercado, S. Sahoo, M. Franz, *Phys. Rev. Lett.* **2022**, *128*, 137002.
- [29] L. R. Cadorim, E. Sardella, M. V. Milošević, *ArXiv Preprint arXiv:2206.14937* **2022**.
- [30] O. Can, T. Tummuru, R. P. Day, I. Elfimov, A. Damascelli, M. Franz *Nat. Phys.* **2021**, *17*, 519-524.
- [31] P. A. Volkov, S. Y. F. Zhao, N. Poccia, X. Cui, P. Kim, J. Pixley, *ArXiv Preprint arXiv:2108.13456* **2021**.
- [32] L. Wang, I. Meric, P. Huang, Q. Gao, Y. Gao, H. Tran, T. Taniguchi, K. Watanabe, L. Campos, D. Muller, J. Guo, P. Kim, K. L. Shepard, C. R. Dean, *Science* **2013**, *342*, 614-617.
- [33] S. Ghosh, J. Vaidya, S. Datta, R. P. Pandeya, D. A. Jangade, R. N. Kulkarni, K. Maiti, A. Thamizhavel, M. M. Deshmukh. *Adv. Mater.* **2020**, *32*, 2002220.
- [34] X. G. Qiu, *Elsevier* **2011**.
- [35] J. Wen, Z. Xu, G. Xu, M. Hucker, J. Tranquada, G. Gu, *J. Cryst. Growth* **2008**, *310*, 1401-1404.
- [36] H. Kao, J. Kwo, H. Takagi, B. Batlogg, *Phys. Rev. B* **1993**, *48*, 9925.
- [37] K. Schlenga, G. Hechtfisher, R. Kleiner, W. Walkenhorst, P. Mueller, H. Johnson, M. Veith, W. Brodkorb, and E. Steinbeiss, *Phys. Rev. Lett.* **1996**, *76*, 4943.
- [38] M. Itoh, S.-i. Karimoto, K. Namekawa, M. Suzuki, *Phys. Rev. B* **1997**, *55*, R12001.
- [39] A. Irie, S. Heim, S. Schromm, M. Möhle, T. Nachtrab, M. Godo, R. Kleiner, P. Müller, G. Oya, *Phys. Rev. B* **2000**, *62*, 6681.
- [40] A. Barone, G. Paterno, Wiley Online Library **1982**, *1*.
- [41] O. Chana, A. Kuzhakhmetov, P. Warburton, D. Hyland, D. Dew-Hughes, C. Grovenor, R. Kinsey, G. Burnell, W. Booij, M. Blamire, R. Kleiner, P. Müller, *Appl. Phys. Lett.* **2000**, *76*, 3603-3605.
- [42] S. Zybtshev, V. Y. Pokrovskii, I. Gorlova, Y. I. Latyshev, V. Luchinin, A. Y. Savenko, *J. Low Temp. Phys.* **2005**, *139*, 281-288.
- [43] J. Schrieffer, J. Wilkins, *Phys. Rev. Lett.* **1963**, *10*, 17.
- [44] K. Schlenga, R. Kleiner, G. Hechtfisher, M. Möhle, S. Schmitt, P. Müller, C. Helm, C. Preis, F. Forsthofer, J.

Keller, H. L. Johnson, M. Veith, E. Steinbeiß, *Phys. Rev.*

B **1998**, *57*, 14518.

[45] E. L. Wolf, *oup Oxford* **2011**, 152.